Polymer Chemistry

Accepted Manuscript

ROYAL SOCIETY OF CHEMISTRY

www.rsc.org/polymers

Unveiling the Hyperbolic Thermal Behavior of poly(*p*-phenylene alkylene)s

*Nicolas F. Sauty, Lucas Caire da Silva, Caitlyn Gallagher, Robert Graf[‡] and Kenneth B. Wagener**

The George and Josephine Butler Polymer Research Laboratory, Department of Chemistry and Center for Macromolecular Science and Engineering, University of Florida, Gainesville, FL 32611-7200

[‡] Max Planck Institute for Polymer Research, Ackermannweg 10, 55128 Mainz, Germany

Abstract: *A series of poly(p-phenylene alkylene)s with methylene run lengths ranging from 8 to 40 were obtained by ADMET polymerization of symmetrical α,ω-diene monomers and subsequent exhaustive hydrogenation. ADMET polymerizations were conducted using dibenzyl carbonate as solvent for the first time, providing materials with high molecular weights as compared with those obtained in standard solvent-free conditions. The thermal properties of both the unsaturated and saturated series were investigated. Poly(p-phenylene alkylene)s exhibit an unprecedented thermal behavior when considering the fusion temperature as a function of the number of methylene spacers. Solid state ^{1}H MAS and ^{1}H-^{13}C correlation experiments demonstrated that the melting behavior is marked by the gradual disruption of the ring π-π interactions with increasing methylene chain length. The higher crystallization tendency of longer alkyl chains was detected by the characteristic broadening of the corresponding solid-state ^{1}H NMR signals and explains the observed increase in melting temperature with the methylene chain length.*

INTRODUCTION

Poly(*p*-phenylene alkylene)s (**PPPz**) are well-defined hydrocarbon polymers consisting of alternating rigid (phenyl) and flexible (alkyl) segments (Figure 1).

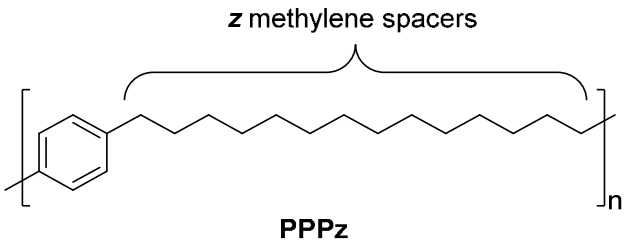

Figure 1. Structure of poly(*p*-phenylene alkylene)s.

Also categorized as precision polymers, poly(*p*-phenylene alkylene)s are highly ordered materials with a functionality placed at perfectly unvarying intervals. Poly(*p*-xylylene) (**PPP2**),[1] otherwise commercially known as Parylene N™, is the only polymer of the series utilized in industrial applications[2] because of its outstanding structural,[3] thermal,[4] and mechanical properties.[5] However, its high aromatic content and limited overall flexibility, make **PPP2** intractable, restricting its processability by common methods.[6] It is generally processed by chemical vapor deposition.[7]

Despite their rather simple structures, only a few poly(*p*-phenylene alkylene)s have been prepared to date. In concept, their properties should range from that of the rigid and intractable poly(*p*-phenylene) to that of the flexible, versatile and highly processable polyethylene. Cramer and co-workers[8] , and Brown and Farthing[9] reported the synthesis of poly(*p*-phenylene octylene)

(**PPP8**); Steiger et al[10] designed a synthetic pathway to poly(*p*-phenylene alkylene)s relying on ADMET polymerization. Among others, poly(*p*-phenylene butylene) (**PPP4**), poly(*p*-phenylene hexylene) (**PPP6**), and **PPP8** were successfully synthesized and fully characterized.[11] When considering the series with an even number of methylene spacers from **PPP2** (T_m = 424 °C) to **PPP8** (T_m = 90 °C), a linear relationship between the frequency of the aromatic moiety and the melting temperature of the polymer was reported.[12]

While this early model was valid for up to 8 methylene units, it did not account for the limit case of linear polyethylene (**PPP**∞) which displays a melting transition at 134 °C. Evidently, the relationship between phenylene frequency and melting temperature is more complex and features at least one local minimum. With the intention of elucidating the influence of the aromatic moiety on thermal behavior, we herein report the investigation of poly(*p*-phenylene alkylene)s containing up to 40 methylene spacers between two consecutive aromatic segments.

RESULTS AND DISCUSSION

Monomer Synthesis. In most symmetrical ADMET monomers, the olefin moieties are installed with the use of α,ω-alkenyl bromides.[13] Given the highly nonpolar character of the desired monomers, we avoided direct routes (for instance, Kumada coupling) for purification purposes. Also, transition metal complexes were avoided to preclude partial isomerization of the α-olefins; should isomerization occur an "ill-defined" material would result. Thus, our two-step route to the monomers involving a benzylic diol was implemented (Figure 2).

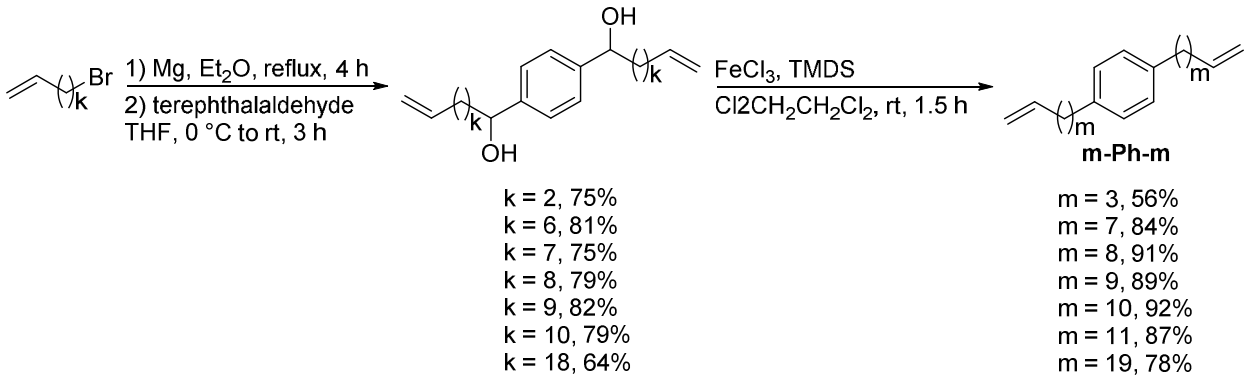

Figure 2. Convenient route to the monomers.

The synthesis of 1,4-di(dodec-11-en-1-yl)benzene (**10-Ph-10**) is representative of the methodology. The 11-bromoundec-1-ene starting material was reacted with magnesium, and the resulting Grignard reagent was added to a THF solution of terephthalaldehyde to give the corresponding benzylic diol in 82% yield. The intermediate was reductively deoxygenated by changing polymethylhydrosiloxane to 1,1,3,3-tetramethyldisiloxane in the procedure published by Chan et al,[14] affording the ADMET monomer **10-Ph-10** in 92% yield.

Across the series, both reactions afforded the desired products in good yields. However, the lack of solubility of the intermediates with 18- and 19-carbon long alkyl chains made their synthesis and subsequent purification particularly difficult, hence the lower yields. Overall, this 2-step process provides higher overall yields than the previously reported 1-step process. An extensive series of monomers possessing 3, 7, 8, 9, 10, 11, and 19 methylene spacers between the aromatic and olefin moieties were synthesized.

Dibenzyl Carbonate as ADMET Polymerization Medium. ADMET polymerizations under bulk conditions have led to polyolefins having number average molecular weights up to 50,000

g/mol, especially when catalyzed with Schrock-Mo; smaller values were usually observed with ruthenium-based catalysts.[15]

Most ADMET polymerizations are conducted at temperatures from 25 °C to about 80 °C.[16] These temperatures are insufficient for the small molecule condensate (usually ethylene) to efficiently overcome the mechanical resistance resulting from formation of the highly viscous polymer, and part of the condensate remains trapped in the polymer matrix. In order to achieve high molecular weights, the small molecule condensate must be continuously evacuated from the reaction vessel, driving the reaction forward. For this reason, most ADMET reactions are performed under high vacuum. Plenio investigated the use of high boiling solvents as ADMET media (such as 1,2-dichlorobenzene), and demonstrated superior condensate removal to form high molecular weight materials.[17] The presence of high boiling solvents precludes use of high vacuum, as the solvent eventually vaporizes.

Organic carbonates (most commonly dimethyl carbonate) have been used as solvents for metathesis reactions,[18] and are almost as effective as the most common metathesis solvent, methylene chloride.[19] However, to the best of our knowledge, no ADMET reactions in organic carbonates have been reported previously. Dibenzyl carbonate (**DBC**) was selected for its high boiling temperature (180-190 °C at 2mmHg), and aromatic content. **DBC** was synthesized from benzyl alcohol and 1,1'-carbonyldiimidazole in 81% yield.

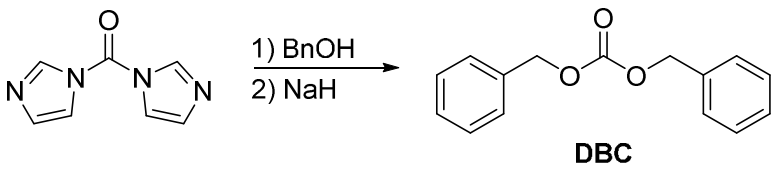

DBC

Figure 3. Synthesis of dibenzyl carbonate.

Monomer **10-Ph-10** (500 mg) was polymerized using **DBC** (5 g) for comparison with the bulk method. The diene monomer was dissolved in **DBC**. The polymerization was conducted using Grubbs' first generation catalyst (1 mol%; 0.5 mol% at t_0 and 0.5 mol% after 24 h) at 80 °C for 48 hours under full vacuum. At the polymerization temperature, the polymer appeared as a translucent sphere which became opaque upon cooling. The resulting unsaturated polymer was found to have a molecular weight of 65,000 g/mol.

This approach was compared to the more traditional bulk polymerization technique. Diene **10-Ph-10** was polymerized in bulk using Grubbs' first generation catalyst (2 mol%; 1 mol% at t_0 and 1 mol% after 24 h) at 50 °C for 48 hours under full vacuum. Shortly after addition of the catalyst, the mixture thickened and solidified into a brittle solid, preventing magnetic stirring. The resulting polyolefin had a number average molecular weight of 20,000 g/mol.

The polymer prepared in **DBC** was found to be qualitatively sturdier than that prepared in bulk, and this observation was supported by GPC analysis, In comparison with bulk conditions, the use of **DBC**, in conjunction with a higher temperature, and half the load of catalyst, tripled the molecular weight of the polyolefin.

All monomers were polymerized under the aforementioned **DBC** conditions. As shown in Table 1, degrees of polymerization ranging from 123 to 219 were obtained across the series. No GPC data could be obtained for **P-19,19** due to its insolubility in organic solvents. However, its film-forming capability provided evidence of high molecular weight. Additional characterization data are presented in Table 1.

Table 1. Characterization of ADMET polyolefins.

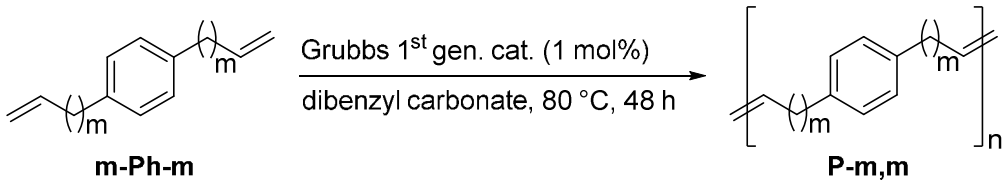

m-Ph-m **P-m,m**

Entry	Polymer (**P-m,m**)	$\overline{M_n}$[a] (g/mol)	$\overline{M_w}$[a] (g/mol)	PDI[a]	$\overline{DP_n}$[a]	T_g[b] (°C)	T_m[b] (°C)	ΔH_m[b] (J/g)	$T_{95\%}$[c] (°C)	$T_{50\%}$[c] (°C)
1	**P-19,19**	n/a	n/a	n/a	n/a	-13	88	115	390	416
2	**P-11,11**	88,000	157,000	1.78	214	-38	74	71	392	416
3	**P-10,10**	65,000	109,000	1.68	167	-40	67	55	391	414
4	**P-9,9**	78,000	123,000	1.58	219	-44	63	56	391	415
5	**P-8,8**	50,000	100,000	2.00	154	-43	60	58	387	412
6	**P-7,7**	55,000	125,000	2.30	183	-51	45	47	380	411
7	**P-3,3**	24,000	61,000	2.56	123	-36	61	18	228	401

[a]GPC in THF as 40 °C. [b]DSC analysis at 5 °C per minute. [c]TGA analysis at 5 °C per minute.

Exhaustive Hydrogenation. The above poly(*p*-phenylene alkylene)s were anticipated to be poorly soluble in most organic solvents at moderate temperatures. As a result, all polyolefins were exhaustively hydrogenated under diimide conditions (140 °C), ensuring no premature precipitation and completion of the reaction. The success of the methodology afforded a series of poly(p-phenylene alkylene)s with alkyl segments containing from 8 to 40 methylene units (Figure 4). The characterization data are provided in Table 2.

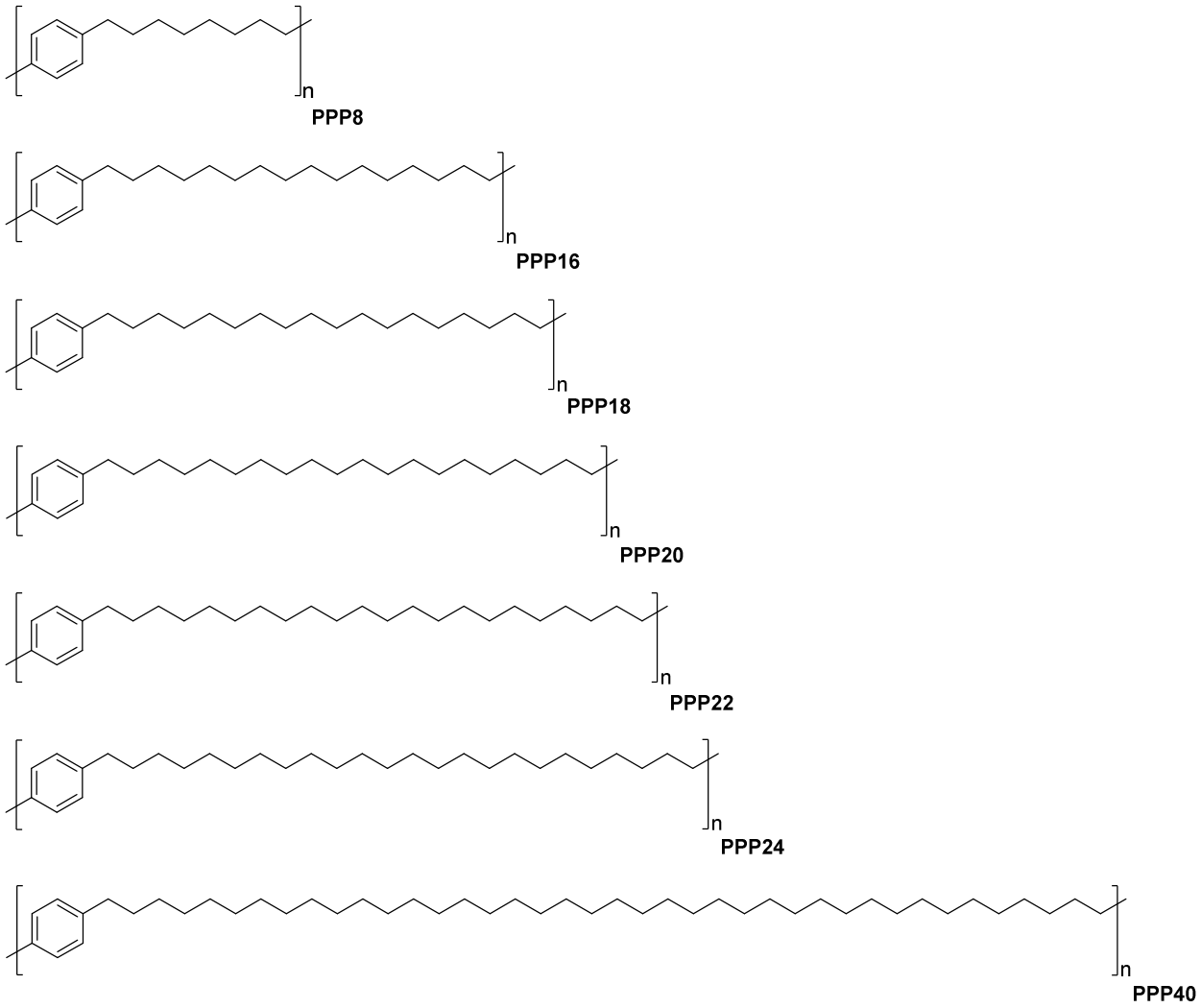

Figure 4. Repeat units in the poly(*p*-phenylene alkylene)s series.

Table 2. Thermal Characterization of poly(*p*-phenylene alkylene)s.

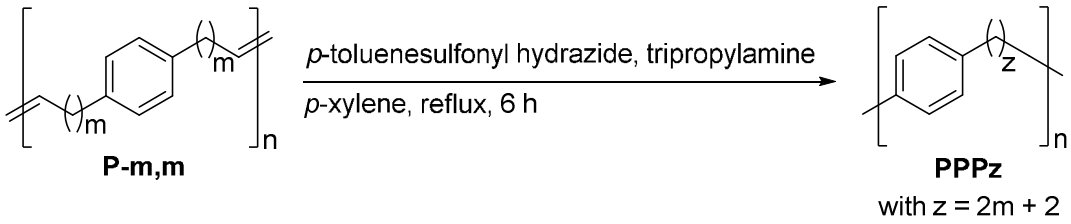

Entry	Polymer	T_g (°C)	T_m (°C)	ΔH_m (J/g)	$T_{95\%}$ (°C)	$T_{50\%}$ (°C)
1	**PPP40**	-8	107	148	389	418
2	**PPP24**	-7	101	108	383	418
3	**PPP22**	-7	101	100	389	419
4	**PPP20**	-11	101	98	386	418
5	**PPP18**	-14	99	98	393	419
6	**PPP16**	-23	96	78	374	417
7	**PPP8**	-31	85	73	389	414

High temperatures are known to promote olefin isomerization during the polymerization when using ruthenium-based catalysts. Additives such as benzoquinones,[20] monophenyl phosphoester,[21] or boron-containing Lewis acids[22] have been reported to greatly minimize or completely suppress this problem. We believe **DBC** serves this purpose as well, given that NMR analysis revealed no extra signals corresponding to a longer- or shorter-than-expected methylene run length in the saturated polymers. For example, the ^{13}C NMR of **PPP8** contains only 4 sharp signals (overlap of two peaks at approximately 29.5 ppm) for the aliphatic carbons (Figure 5).

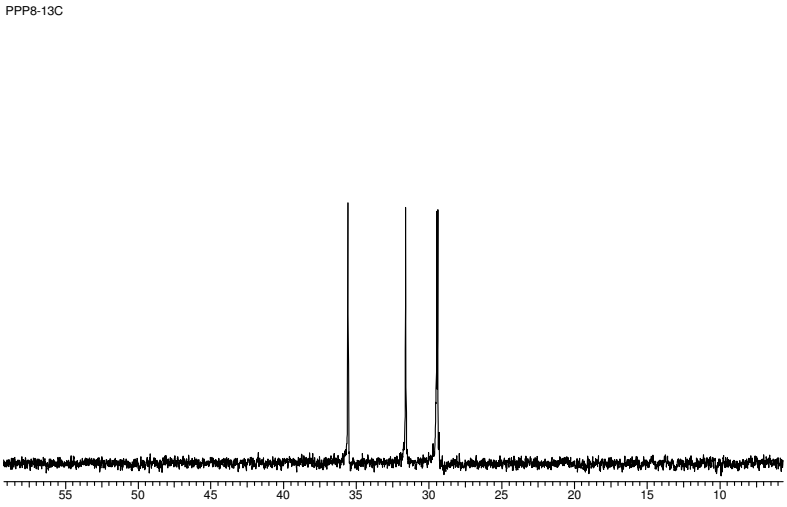

Figure 5. ^{13}C NMR of the aliphatic region of **PPP8.**

Figure 6 shows the typical progression observed through ^{1}H NMR from monomer, to polyolefin and finally to saturated precision polymer. This exemplifies both the high conversion of monomer terminal double bonds into internal olefins in the ADMET polymer and the subsequent complete hydrogenation of the aforementioned polymer under diimide conditions.

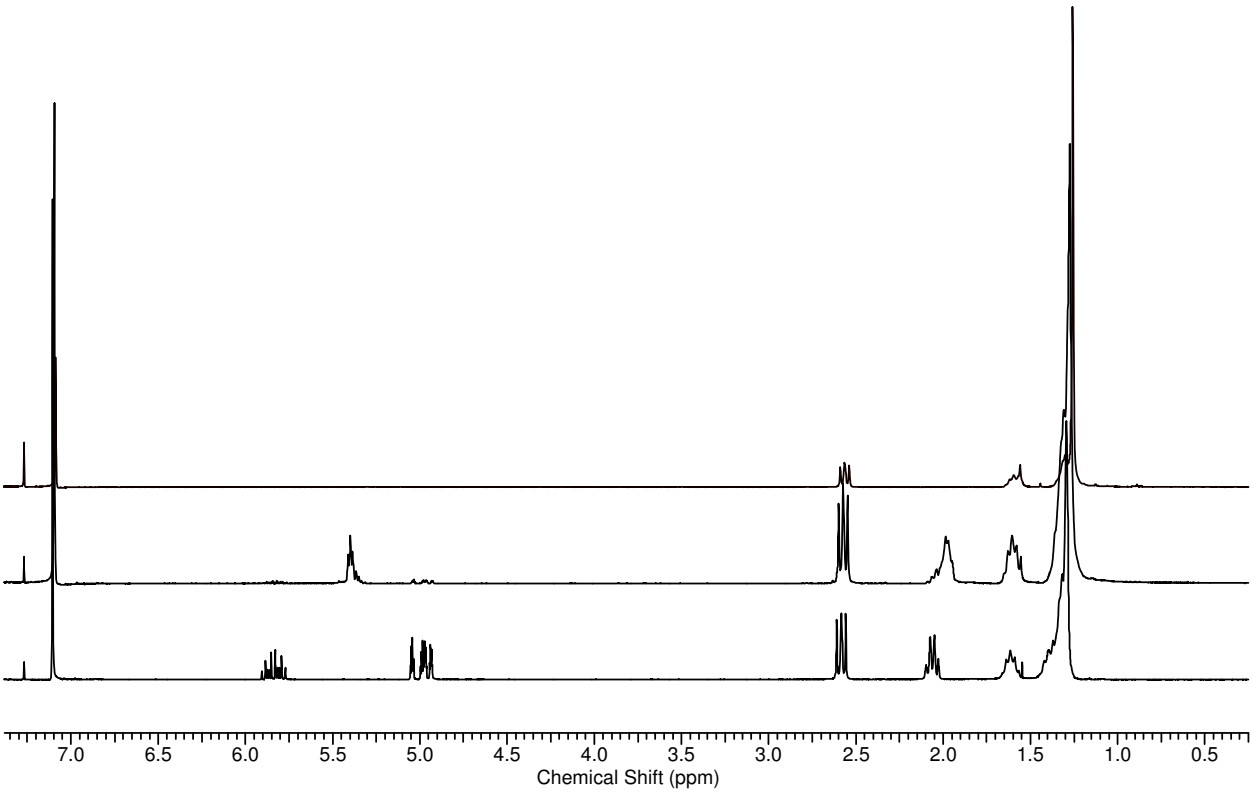

Figure 6. ^{1}H NMR Spectra of the monomer **10-Ph-10** (bottom), unsaturated polyolefin **P10,10** (middle), and poly(*p*-phenylene docosylene) **PPP22** (top).

Thermogravimetric Analysis (TGA). Consistent degradation temperatures were observed for all unsaturated and saturated polyolefins with $T_{95\%}$ around 385 °C and $T_{50\%}$ around 415 °C. However, **P-3,3** exhibited a dissimilar $T_{95\%}$ while maintaining a consistent $T_{50\%}$, suggesting a different thermal degradation pathway for this polymer. A typical example is shown in Figure 7.

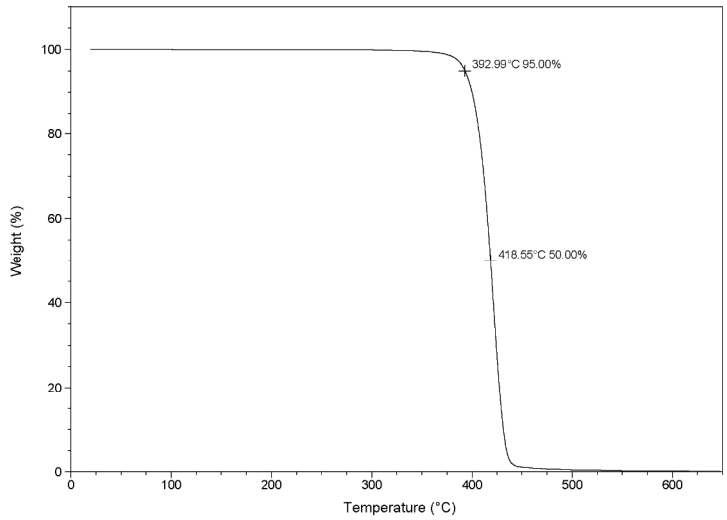

Figure 7. Typical TGA trace (**PPP18**).

Differential Scanning Calorimetry (DSC) Analysis of the unsaturated ADMET polymers. Consistent with other precision polymers, glass transition and melting temperatures increased with increasing methylene content. A similar trend was observed for the enthalpy of melting, indicating a higher crystallinity content with lower aromatic frequency. The increase in melting temperature with the methylene run length is consistent with the longer methylene sections available for crystallization during the formation of the lamella. This behavior has also been observed in ethylene/α-olefin copolymers with alkyl branches placed at exact intervals along the methylene backbone.[23,24,25] As shown by previous studies on semicrystalline polymers, the degree of crystallization also affects the glass transition temperature through the confinement of the amorphous regions caused by the rigid lamella.[26,27,28] The higher fraction of crystalline regions contributes to a more effective restriction of the segmental motions in the amorphous phase shifting the glass transition to higher temperatures**.**

Differential Scanning Calorimetry Analysis of Poly(*p*-phenylene alkylene)s. Across the series of poly(*p*-phenylene alkylene)s, the melting temperature increased with increasing methylene content, as shown in Figure 8.

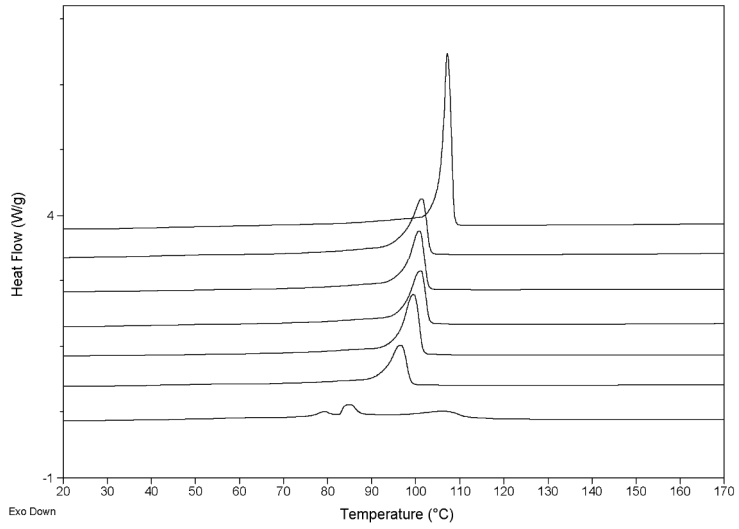

Figure 8. DSC analysis of poly(*p*-phenylene alkylene)s. Bottom to top: **PPP8**, **PPP16**, **PPP18**, **PPP20**, **PPP22**, **PPP24**, and **PPP40**.

The melting temperature increases from 85 °C (8 methylene units) to 104 °C (40 methylene units), suggesting a minimal influence of the methylene run length in these polymers. Combining our results with existing data provides a series of poly(*p*-phenylene alkylene)s with methylene contents ranging from 2 to 40. This greatly extended series is characterized by a bitonic behavior. While a plot of the melting temperature as a function of methylene run length does not reveal a clear pattern, a plot of the melting temperature as a function of the multiplicative inverse of the methylene run length displays two linear segments (Figure 9), representing the asymptotes of a hyperbola (Equation 1). The experimental data points were

utilized to determine the parameters of this empirical relationship ($a = 123\ °C; b = 323\ °C; c = 234\ °C;\ z_0 = 8$) via least squares methodology.

$$T_m(z) = \sqrt{1 + a^2\left(\frac{1}{z} - \frac{1}{z_o}\right)} + b\left(\frac{1}{z} - \frac{1}{z_o}\right) + c \qquad (1)$$

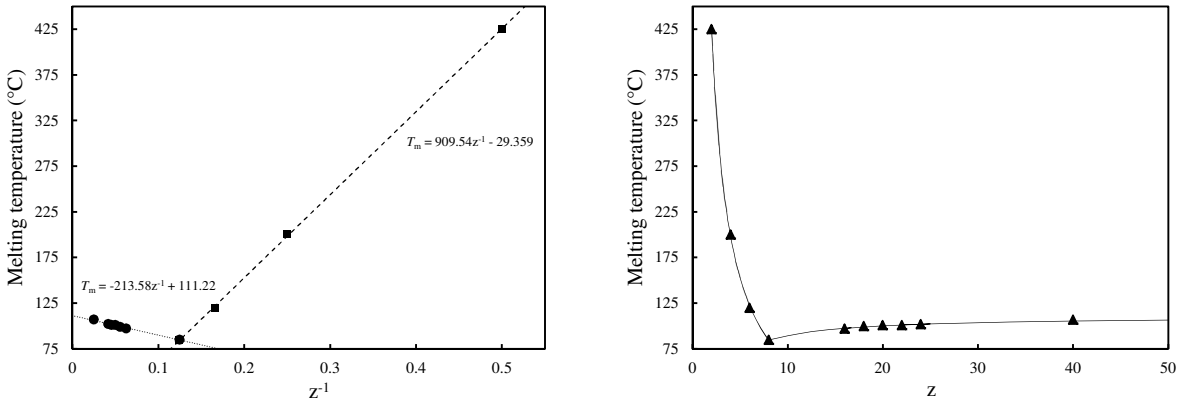

Figure 9. (left) Melting temperature as a function of the multiplicative inverse of the methylene run length (●: this work; ■: previously reported data; dotted line: linear regression on this work; dashed line: linear regression on previously reported data). (right) Melting temperature as a function of the methylene run length (previously reported work and present data).

In crystalline or semi-crystalline materials, disturbance of the crystal lattice by impurities or structural defects results in a decrease in the required energy to disrupt the lattice, thereby lowering the melting transition. In the present case, the phenylene moieties prevent efficient packing of the flexible methylene segments, and the methylene segments prevent efficient packing of the phenylene groups. In polymers such as polyethylene terephthalate and nylon, which are stabilized by dipole-dipole and hydrogen bonding interactions, respectively, the temperature drop is much less significant. Thus, the melting temperature remains above that of polyethylene for any methylene spacer length in polyethylene terephthalate or Nylon, due to the

cohesive forces provided by polar interactions. In the case of poly(*p*-phenylene alkylene)s, the fact that the melting temperature drops 50 °C below that of polyethylene can be interpreted in two different ways. First, it could be the evidence that there are no cohesive forces capable of counteracting the crystal lattice disturbance; i.e., in other words, minimal or null π-π interactions. Second, the preferential aromatic interactions leading to the formation of off-center or edge-to-face (T-shaped) aromatic clusters prevents efficient packing of the methylene sections, eventually leading to a weak crystalline structure resulting in a low melting transition.

Previous studies on semi-crystalline polymers containing alkyl branches at precise intervals along the chain shows that inclusion of branches into the crystalline phase is determined by the branch size. One important general conclusion from such studies is that bulky side groups are excluded from the lamellae while less sterically demanding groups can be incorporated depending on the crystallization conditions. Branch exclusion can be confirmed by the characteristic "paraffin-like" x-ray diffraction pattern due to crystallization of unperturbed alkyl chains.[15]

A preliminary analysis of the powder diffraction pattern obtained from PPP could not unequivocally confirm the presence of the "paraffin-like" structure that supports the ring exclusion model. In fact, no correlation could be found between the methylene chain length and diffraction patterns of **PPP**. A complete analysis of the complex crystalline structure in **PPP** will be the subject of a future publication.

A different strategy to understand the reorganization of the crystalline phase and, consequently, the underlying mechanism that modulate the melting behavior is to detect variations of local intermolecular interactions via solid-state NMR. In the following, we

demonstrate that the melting behavior involves a complex balance between the disruption of aromatic ring-ring interactions and the optimization of the intermolecular van der Waals forces between methylene chains.

Solid State NMR Analysis. The changes in local intermolecular interactions in **PPP** as a function of the methylene run length can be studied by solid state NMR. The local structural reorganizations involving phenylene rings and alkyl chains as a function of methylene chain length can be detected by the corresponding changes in the solid-state NMR spectrum. Molecular packing in poly(*p*-phenylene alkylene)s was investigated by solid state ^{1}H MAS NMR and REPT-HSQC NMR (Recoupled Polarization Transfer - Heteronuclear Single Quantum Correlation). The latter technique combines fast MAS with a REDOR recoupling scheme that provides selective heteronuclear dipolar recoupling for ^{1}H-^{13}C correlation with efficient ^{1}H homonuclear dipolar decoupling, resulting in high resolution 2D correlation spectra. [29,30]

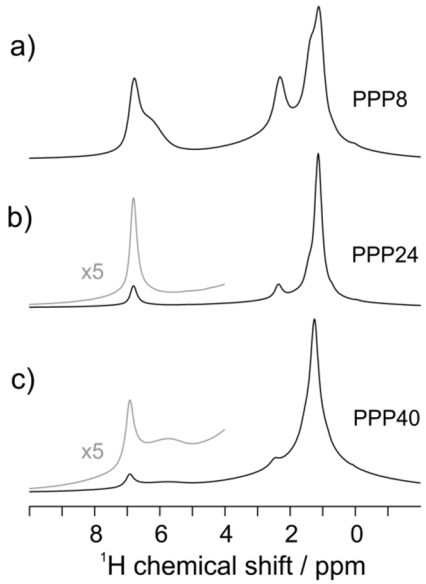

Figure 10. ^{1}H MAS solid-state NMR spectra of **PPP8**, **PPP24** and **PPP40** recorded at 50°C, 25 kHz MAS and 700.23 MHz ^{1}H Larmor frequency. The grey lines in b) and c) show 5 fold magnifications of the signal intensities in the aromatic region.

Figure 10 shows the ^{1}H MAS NMR spectra recorded in the solid state of poly(*p*-phenylene alkylene)s samples with different methylene spacing. In **PPP8** (Figure 10a), the aromatic signal at 6.8 ppm in the ^{1}H MAS NMR shows a clear shoulder at higher frequency. This high field shift is observed exclusively in the solid state and is attributed to intermolecular electronic shielding caused by ring currents from adjacent phenylene units. Similar shifts in the proton frequency have been observed in other aromatic systems displaying π-π stacking, such as hexabenzocoronene and poly-3-hexyl-thiophene.[31,32,33] The absence of π-π stacking in **PPP24** suggests that, compared to **PPP8**, the increased methylene run length is sufficient to disrupt the intermolecular interaction between adjacent phenylene units. Remarkably, for **PPP40** a second signal due to π-π stacking of the phenylene rings is observed, with an even more pronounced high field shift of the aromatic signal compared to **PPP8**.

This finding for **PPP40** suggests that the spatial proximity of phenylene rings in **PPP8** results most likely from the higher density of randomly distributed phenylene rings. In contrast, the π-π stacked phenylene rings in **PPP40** seem to have an inherent denser packing, causing a more pronounced π shift.

Further structural details are given by the 2D correlation spectra in Figure 11.[34] The aliphatic ^{13}C region of the correlation spectrum of **PPP8**, **PPP24** and **PPP40** (right part of Figure 11 b), c) and d)) shows correlations between the aliphatic carbons and the directly bonded protons. For **PPP8** and **PPP24**, the only difference in this region is the substantially wider ^{1}H

line width of the alkyl chains (site 5) in **PPP24**. This indicates a reduced mobility of the alkyl chains in **PPP24**, suggesting a more pronounced crystallization tendency of the alkyl segments. The aliphatic region of the correlation spectrum of **PPP40** is completely dominated by the signals of the long alkyl chains between neighboring phenylene rings. The signal intensity of sites close to the phenylene rings are very close to the noise level, and therefore not suitable for the analysis of the local molecular packing arrangement.

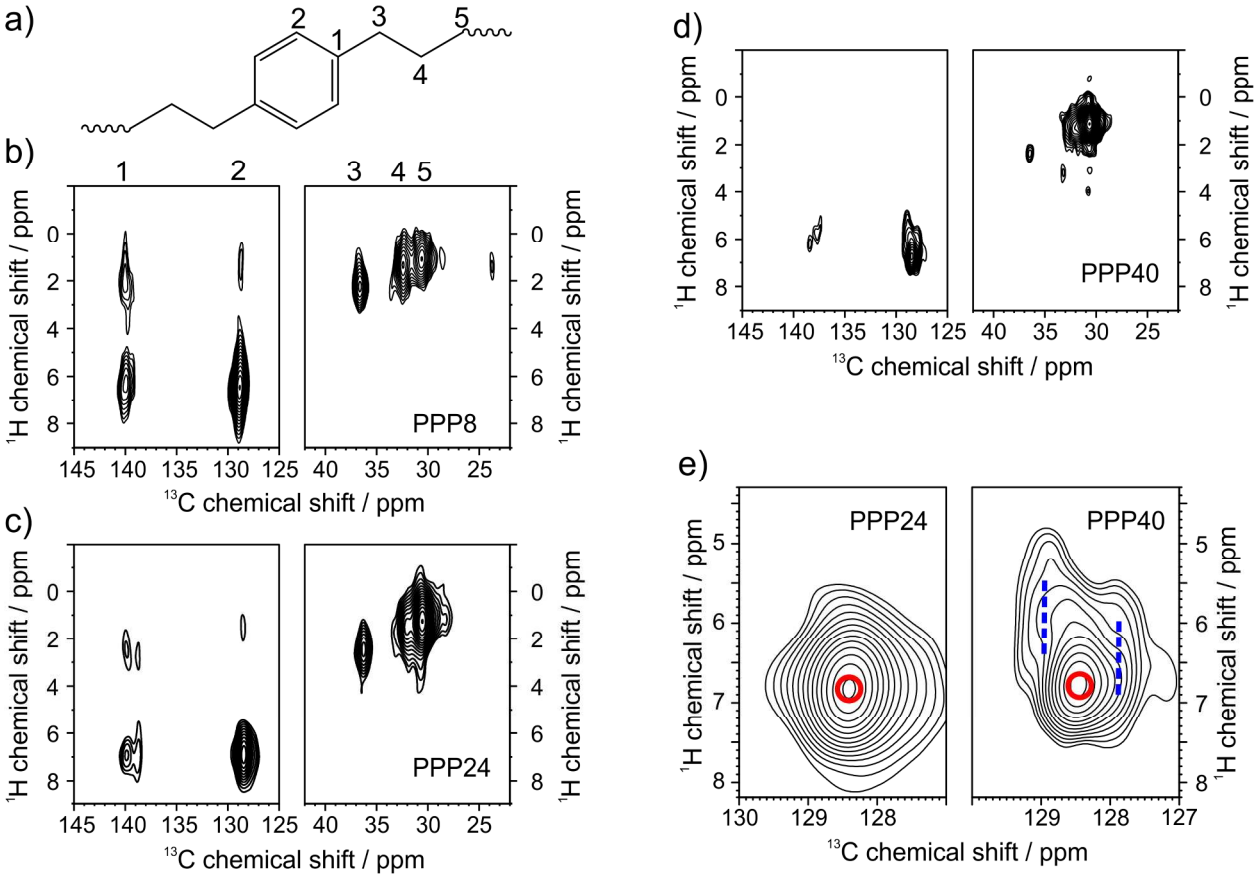

Figure 11. ^{13}C{^{1}H} REPT HSQC solid-state NMR spectra of **PPP8** (b) , **PPP24** (c)) and **PPP40** (d) recorded at 25 kHz MAS, 700 MHz ^{1}H Larmor frequency and 50°C sample temperature with 4 rotor periods hetero nuclear dipolar recoupling for excitation and reconversion. In part a) a scheme of the chemical structure is given for the assignment of the ^{13}C NMR signals. (e) shows a zoom of the signals of the protonated phenylene sites in **PPP24** and **PPP40**.

More significant differences between the samples, however, are observed in the aromatic region of the correlation spectra (left part of Figure 11 b), c) and d)). As the methylene run length increases from 8 to 24, one observes a splitting of the quaternary carbon (C1) signal and a significant broadening of the methine carbon (C2) in the ^{13}C dimension. A similar splitting of a quaternary ^{13}C signal has been observed previously in poly(*p*-xylylene) and has been attributed to variations in the molecular packing imposed by the polymorphism displayed by this material.[35] Upon increasing of the alkyl chain length between neighboring phenylene rings to 40 CH_2 groups, not only does the quarternary (C1) carbon signal show a splitting, but the methine (C2) carbon signal shows a splitting in the ^{13}C dimension as well, together with a significant high field shift in the ^{1}H dimension for phenylene units close to crystalline alkyl chains, as indicated by the dashed blue lines in Figure 11e). Methine signals from non-crystalline regions of **PPP40** are observed at the same chemical shift values for ^{1}H and ^{13}C as the dominating methine signal in **PPP24**.

The observed line shape of the $^{13}C\{^{1}H\}$ methine correlation signal is attributed to the increased concentration of phenylene rings in the interphase between crystalline alkyl chains and non-crystalline regions. This induces an ordering of the phenylene rings at the interphase with significantly reduced molecular mobility compared to phenylene moieties in non-crystalline regions of the material. The increased density of phenylene rings induces intermolecular shifts of NMR signals due to the so-called ring current effects, which depend on the orientation of an observed nuclear spin relative to the π electron system of a phenylene ring. This may explain the overall shifts in the ^{1}H dimension relative to the value of the signals from non-crystalline regions. On the other hand, the observation that the splitting in the ^{13}C dimension is symmetric to

the chemical shift value observed for methine sites in non-crystalline areas cannot be explained by the ring current effect, and results from the relative orientation of the phenylene ring to the crystalline all-trans alkyl chain. The energetic minimum for a single chain conformation of a phenylene ring in an alkyl chain is obtained when the next-nearest C-C bond to the phenylene ring has a dihedral angle of 90° to the phenyl plane. In this case, the methine sites next to this bond would be equivalent. In contrast, when the next-nearest C-C bond is coplanar with the phenylene ring, one of the methine sites would be *trans* to this bond, whereas the other methine site would be *cis*, giving rise to a different chemical shift. Because the relative orientation of the next-nearest C-C bond relative to the phenyl plane causes only a redistribution of electron density in the aromatic system, the induced shift differences would be symmetric around the average or equilibrium position, which is observed in the non-crystalline region. Remarkably, the ^{1}H chemical shifts for split ^{13}C signals do not match because the conformational splitting of the ^{13}C signals shows only a negligible influence on ^{1}H chemical shifts. Most likely, the two distinct methine sites of the phenylene rings are arranged in the interphase, such that methine sites with higher *cis* character experience a weaker low field shift due to ring currents of neighboring phenylene rings compared to the methine sites with higher *trans* character. Thus the ^{13}C{^{1}H} REPT-HSQC spectrum of **PPP40** nicely confirms the formation of a highly ordered, phenylene rich interphase on top of crystalline alkyl layers.

The question, as to why the same behavior was not be observed in the REPT-HSQC spectrum of **PPP24,** even though a clear crystallization peak of the alkyl chains is observed in the DSC trace for **PPP24,** can be explained by revisiting the REPT-HSQC spectrum of **PPP24**, keeping the findings from **PPP40** in mind. In **PPP24**, The asymmetric peak shape indicated by the lowest contour levels, which is lost going to higher contour levels, suggests that initial

tendencies for the formation of an ordered phenylene interphase are present in **PPP24**. However, the signal is dominated by the contribution from non-crystalline regions, indicating that the interphase is still too mobile and not sufficiently ordered to be stable on the NMR time scale.

Randomization. Loss of the precise spacing of the phenylene groups was introduced by copolymerization of **3-Ph-3** with 1,9-decadiene in a 1 to 4 molar ratio, respectively, followed by exhaustive hydrogenation yielding an "ill-defined" polymer having 40 methylene spacers on average. Because a small portion of the 1,9-decadiene vaporized during the polymerization, the final polymer was found to have an average of 36.9 methylene spacers between each aromatic moiety, as determined via ^{1}H NMR analysis. As shown in Table 3, the melting temperature of the resulting random material was similar to that of **PPP40**, but the heat of fusion was four fifths that of **PPP40**. This observation is not unusual and indicates less order in the polymer matrix.

Table 3. Randomization study.

Entry	Polymer	1,9-Decadiene fraction	T_g (°C)	T_m (°C)	ΔH_m (J/g)
1	**PPP40**	n/a	-8	107	148
2	**PPP36.9***	3.61	n/a	105	118

Simulated Isomerization. Isomerization, resulting from either partially isomerized monomers, or a side-reaction during the polymerization, inevitably leads to ill-defined structures with altered

thermal properties, which reflect the extent of imperfection. With the intention of evaluating the influence of isomerization on thermal properties, a series of **9-Ph-9** and **10-Ph-10** copolymers were prepared. In this model, **9-Ph-9** is the isomerized analog of **10-Ph-10**, as shown in figure 12.

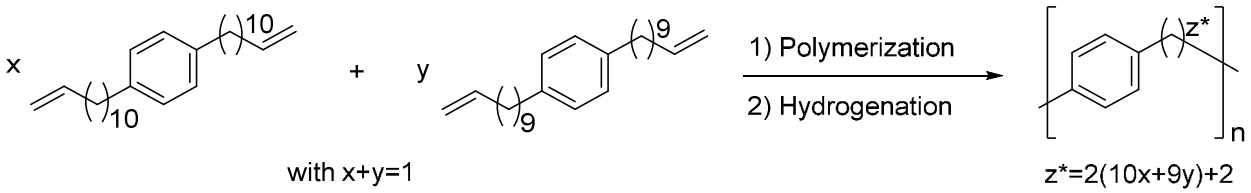

Figure 12. Simulated isomerization.

Polymers having 21.98, 21.90, and 21 methylene spacers on average between each phenylene unit resulted from incorporating 1%, 5%, and 50% of **9-Ph-9** with **10-Ph-10**, respectively, and the characterization data are shown in Table 4. A depression of the melting transition was observed with increasing **9-Ph-9** content with a minimum value of 91 °C for 50% isomerization, corresponding to a 10 °C drop when compared to the precise **PPP20** and **PPP22**. This last point demonstrates the ability to observe a continuous average "odd-even" effect. The glass transition temperature was minimally affected by the structural imperfections and diminished with increasing isomerization content.

Table 4. Thermal data from polymers with simulated isomerizations.

Entry	Polymer	Isomerization content (y)	T_g (°C)	T_m (°C)	ΔH_m (J/g)
1	**PPP22**	0%	-7	101	100
2	**PPP21.98***	1%	-9	101	101
3	**PPP21.9***	5%	-10	99	99
4	**PPP21***	50%	-11	91	92
5	**PPP20**	100%	-11	101	98

CONCLUSION

We have established a robust strategy to afford poly(*p*-phenylene alkylene)s having up to 40 methylene units between two consecutive aromatic segments. The monomers, built from terephthalaldehyde and an α,ω-alkenyl bromide, were produced in high yields in two steps. ADMET polymerization was performed in dibenzyl carbonate and yielded high molecular weight polymers. Exhaustive hydrogenation of the ADMET polymers yielded the desired poly(*p*-phenylene alkylene)s. Thermal analysis of our polymers collectively with previously reported data points revealed the bitonic thermal behavior of the series. A hyperbolic behavior was demonstrated and the proposed empirical mathematical description predicts the melting temperatures within ±1°C. This model also suggests that the crystal lattice disruption by the phenylene moiety remains significant even at methylene run lengths greater than 40. As demonstrated by solid state NMR, the increase of the methylene run length changes the crystalline structure in two major ways. One involves the more efficient molecular packing of alkyl chains due to longer methylene segments available during crystallization. The increase in

melting temperature of **PPP(≥8)** with increasing alkyl chain length is therefore caused by the reorganization of the lamellae driven by the optimization of intermolecular interactions between methylene segments in adjacent chains. The second major change in the crystalline structure concerns the aromatic interaction between phenylene rings. Combined results from ^{1}H MAS and ^{1}H-^{13}C correlation solid state NMR demonstrate a tendency towards disruption of the π-π interactions of the rings embedded in the crystalline phase followed by partial expulsion of the phenylene rings as the alkyl chain becomes longer.

Randomization with 1,9-decadiene provided a material with similar melting temperature but with a much lower enthalpy of fusion. The simulated isomerization study underlines the importance of precise placement of the aromatic segment in determining the thermal properties. The resulting polymers strictly behaved as statistical polymers with continuous average "odd-even" effect.

ACKNOWLEDGMENTS

We gratefully acknowledge the National Science Foundation (DMR-1203136), the Army Research Office (W911NF-13-1-0362) and the International Max Planck Research School for Polymer Materials Science at the Max Planck Institute for Polymer Research in Mainz for the financial support of this research. Also, we would like to thank Prof. Dr. Paul Blom and his group for the opportunity and Dr. Dmytro Dudenko for helpful discussion on solid state NMR.

REFERENCES

1 Errede, L. A.; Gregorian, R. S.; Hoyt, J. M. *J. Am. Chem. Soc.* **1960**, *82*, 5218-5223.

2 Bergman, B. R. Parylene Coating of a Tire Component. WO2012134483 (A1), October 4, 2012.

3 Choi, Y.-H.; Lee, G.-Y.; Ko, H.; Chang, Y. W.; Kang, M.-J.; Pyun, J.-C. *Biosensors and Bioelectronics* **2014**, *56*, 286-294.

4 (a) Schaefgen, J. R. *Journal of Polymer Science* **1959**, *41*, 133. (b) Errede, L. A.; Knoll, N. *Journal of Polymer Science* **1962**, *60*, 33. (c) Kirkpatrick, D. E.; Wunderlich, B. *Die Makromolekulare Chemie* **1985**, *186*, 2595.

5 Van der Werff, H.; Pennings, A. *J. Polym. Bull.* **1988**, *19*, 587-594.

6 Szwarc, M. Polym. *Eng. Sci.* **1976**, *16*, 473-479.

7 Gaynor, J. F.; Desu, S. B.; Senkevich, J. J. *Macromolecules* **1995**, *28*, 7343-7348.

8 Cramer, E.; Percec, V. *J. Polym. Sci., Part A: Polym. Chem.* **1990**, *28*, 3029-3046.

9 Brown, C. J.; Farthing, A. C. J. Chem. Soc. 1953, 3270-3278.

10 Steiger, D.; Ehrenstein, M.; Weder, C.; Smith, P. *Macromolecules* **1998**, *31*, 1254-1260.

11 Steiger, D.; Ehrenstein, M.; Weder, C.; Smith, P. *Macromolecules* **1998**, *31*, 1254-1260.

12 Steiger, D.; Tervoort, T.; Weder, C.; Smith, P. *Macromolecular Rapid Communications* **2000**, *21*, 405-422.

13 Rojas, G.; Inci, B.; Wei, Y.; Wagener, K. B. *J. Am. Chem. Soc*. **2009**, *131*, 17376-17386.

14 Chan, L.; Lim, J.; Kim, S. *Synlett* **2011**, *19*, 2862-2866.

15 Inci, B.; Lieberwirth, I.; Steffen, W.; Mezger, M.; Graf, R.; Landfester, K.; Wagener, K. B. *Macromolecules* **2012**, *45*, 3367-3376.

16 Aitken, B. S.; Minjae, L.; Hunley, M. T.; Gibson, H. W.; Wagener, K. B. *Macromolecules* **2010**, *43*, 1699-1701.

17 Weychardt, H.; Plenio, H. *Organometallics* **2008**, *27*, 1479-1485.

18 Schäffner, B.; Schäffner, F.; Verevkin, S. P.; Börner, A. *Chem. Rev.* **2010**, *110*, 4554–4581.

19 Bruneau, C. and Fischmeister, C. (2014) Olefin Metathesis in Green Organic Solvents and without Solvent, in Olefin Metathesis: Theory and Practice (ed K. Grela), John Wiley & Sons, Inc., Hoboken, NJ, USA.

20 Hong, S. H.; Sanders, D. P.; Lee, C. W.; Grubbs, R. H. *J. Am. Chem. Soc.* **2005**, *127*, 17160-17161.

21 Formentín, P.; Gimeno, N.; Steinke, J. H. G.; Vilar, R. *J. Org. Chem.* **2005**, *70*, 8235-8238.

22 Simocko, C.; Wagener, K. B. *Organometallics* **2013**, *32*, 2513-2516.

23 Few, C.; Thompson, D. L.; Wagener, K. B. *Macromol. Rapid Commun.* **2014**, *35*, 123-132.

24 Rojas, G.; Berda, E. B.; Wagener, K. B. *Polymer*, **2008**, *49*, 2985-2995.

25 Zuluaga, F.; Inci, B.; Nozue, Y.; Hosoda, S.; Wagener, K. B. *Macromolecules*, **2009**, *42*, 4953-4955.

26 Atkinson, J. R.; Hay, J. N.; Jenkins, M. J. *Polymer*, **2002**, *43*, 731-735.

27 Mano, J. F.; Gómez Ribelles, J. L.; Alves, N. M.; Salmerón Sanchez, M. *Polymer*, **2005**, *46*, 8258-8265.

28 Hay, J. N. *Pure & Appl. Chem*., **1995**, *67*, 1855-1858.

29 Saalwächter, K.; Graf, R.; Spiess, H. W. *J. Magn. Reson.* **1999**, *140*, 471-476.

30 Saalwächter, K.; Graf, R.; Spiess, H. W. *J. Magn. Reson.* **2001**, 148, 398-418.

31 Brown, S. p.; Schnell, I.; Brand, J. D.; Mullen, K.; Spiess, H. W. *J. Am. Chem. Soc.* **1999**, *121*, 6712-6718.

32 Dudencko, D.; Kiersnowski, A.; Shu, J.; Pisula, W.; Sebastiani, D.; Spiess, H. W.; Hansen, M. R. *Angew. Chem. Int. Ed.* **2012**, *51*, 11068-11072.

33 S. P. Brown, T. Schaller, U. P. Seelbach, et al. Angew. Chem., Int. Ed. Engl., **2001**, 40, 717
34 K. Schmidt-Rohr and H. W. Spiess in *Multidimensional Solid-State NMR and Polymers* Academic Press: New York, **1994**

35 Sroka-Bartnicka, A.; Olejniczak, S.; Ciesielski, W.; Nosal, A.; Szymanowski, H.; Gazicki-Lipman, M.; Potrzebowski, M. J. *J. Phys. Chem. B* **2009**, *113*, 5464-5472.

Graphical Abstract

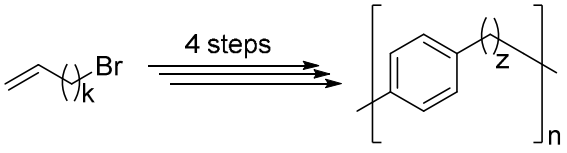

PPPz
with z = 2(k+1)+2